Steel and Composite Structures, *Vol. 33, No. 6 (2019) 877-889*
DOI: https://doi.org/10.12989/scs.2019.33.6.877

Developments of double skin composite walls using novel enhanced C-channel connectors

Jia-Bao Yan [1,2a], An-Zhen Chen [2b] and Tao Wang*[3]

[1] *Key Laboratory of Coast Civil Structure Safety of Ministry of Education, Tianjin University, Tianjin 300350, China*
[2] *School of Civil Engineering, Tianjin University, Tianjin 300350, China*
[3] *Key Laboratory of Earthquake Engineering and Engineering Vibration, Institute of Engineering Mechanics, CEA, Harbin 150080, China*

(*Received August 14, 2019, Revised September 24, 2019, Accepted September 30, 2019*)

Abstract. The developments of double skin composite (DSC) walls with novel enhanced C-channel connectors (DSCW-EC) were reported. Followed axial compression tests on prototype walls were carried to evaluate structural performances of this novel DSC composite structures. The testing program consists of five specimens and focused on the layout of the novel enhanced C-channel (EC) connectors, which include the web direction of C-channels, steel-faceplate thickness, vertical and horizontal spacing of C-channels. Crushing in concrete core and buckling of steel faceplate were two main observed failed modes from the compression tests. However, elastic or plastic buckling of the steel faceplate varies with designed parameters in different specimens. The influences of those investigated parameters on axial compressive behaviors of DSCW-ECs were analyzed and discussed. Recommendations on the layout of novel EC connectors were then given based on these test results and discussions. This paper also developed analytical models for predictions on ultimate compressive resistance of DSCW-ECs. Validation against the reported test results show that the developed theoretical models predict well the ultimate compressive resistance of DSCW-ECs.

Keywords: double skin composite structure; compressive test; shear connectors; composite walls; prototype tests; analytical models; C-channel

1. Introduction

Double skin composite (DSC) structure is a type of relative new structure with a history more than three decades (Sohel and Liew 2014). The main components in this type of structure are a concrete core, two external steel skin plates, and bonding mechanical connectors (or cohesive materials) between the concrete core and two steel skin plates. Compared with reinforced concrete structures, the transparent advantages of this sandwich structure include removal of mould for concrete casting, reduced site work and labour forces, avoiding details of reinforcement, improved permeability, improved construction efficiency, and high resistance subjected to impact and blast loads (Remennikov *et al.* 2019). This type of structure has been widely used in engineering constructions as the immersed tunnels (Lin *et al.* 2018), high-rise-building shear walls (Nie *et al*. 2013, Qin *et al*. 2019a,b), composite beams (Hossain and Wright 2004, Zou *et al.* 2016), shielding walls in nuclear power plant (Varma *et al.* 2014), shield tunnels (Zhang and Atsushi 2010), containment (Sener *et al.* 2015), bridge deck, offshore platform deck, ship hulls (Kosters and Wennhage 2009), and protective structures (Yan *et al.* 2014a, b, Sohel and Liew 2014).

*Corresponding author, Ph.D., Professor,
E-mail: wangtao@iem.ac.cn
[a] Associate Professor, E-mail: ceeyanj@163.com
[b] Master Student

In double skin composite walls (DSCWs), shear connectors act essentially on resisting interfacial slip and out-of-plane separation at the steel-concrete interface (Yan *et al.* 2018, Yan *et al.* 2019a, b). Previous extensive studies showed that various types of shear connectors were developed for DSCWs, e.g., headed studs (Yan *et al.* 2018), friction-welded straight bars (Xie *et al.* 2007), angles (Malek *et al.* 1993), C-channel (Chen *et al.* 2019), laser-welded connectors (Leekitwattana *et al.* 2011, Jelovica *et al.* 2016, Yousefi and Ghalehnovi 2017a, b), wave connectors (Qin *et al.* 2019a, b), and J-hook connectors (Liew *et al.* 2009, Yan *et al.* 2014a, b). These mechanical connectors can be categorized into three types depending on their linking ways, namely indirect, semi-direct, and direct link (Yan *et al.* 2019b). Headed studs, angles, and C-channel are belonged to "indirect link" type of connectors, and their interfacial shear resistance and steel-concrete separation resistance mainly rely on their connector-concrete interactions. Once the concrete core fails, this type of structure tends to lose their composite actions (Yan *et al.* 2018). Friction-welded straight bars in "Bi-steel" structure, laser-welded connectors, and wave connectors are belonged to the "direct link" type of connector. Previous studies proved these connectors offered high structural performance especially on maintaining the structural integrity (Xie *et al.* 2007, Leekitwattana *et al.* 2011, Jelovica *et al.* 2016, Qin *et al.* 2019a, b). However, these two types of welding technologies tend to be much more costing compared with the arch welding or spot welding, which limits their applications in the engineering practice. Moreover, the

http://www.techno-press.org/?journal=scs&subpage=6
ISSN: 1229-9367 (Print), 1598-6233 (Online)

thickness of the "Bi-steel" sandwich structure was limited within 0.2~0.7 m due to the size limitations of welding equipment (Xie *et al*. 2007). The thickness of the steel skin plates was limited to a certain value (usually less than 6 mm) depends on the laser welding machine. J-hook connectors, a typical type of "semi-direct link" connector, improved the steel-concrete separation resistance and offer a good solution to produce slim decking without limitations on the depth of DSC structures (Sohel and Liew 2014). However, J-hook connectors tend to produce assembling difficulties of two steel skin plates since making sure hundreds pairs of J-hook connectors to interlock each other is a big challenge in the engineering practice. Moreover, the fabricating J-hooks through cold-forming produce additional works. Thus, it can be found that it is necessary to develop a new type of "direct link" connectors to improve the steel-concrete bonding for DSCWs. Compressive behaviours of DSCWs adopting this new type of mechanical connectors also need to be evaluated.

This paper firstly developed a new type of mechanical connectors for DSCWs, namely "enhanced C-channel" connectors. Fig. 1 shows the potential application of this novel DSCW. Then, a testing program with five full-scale specimens were performed to evaluate the compressive behaviors of DSCWs with EC connectors. Including these experimental studies, in order to determine the ultimate compressive resistance of this novel DSCW, theoretical models were also developed. Finally, from these tests and analytical works, conclusions were given.

2. Developments of enhanced C-channel connectors

In DSC structures, the main functions of the mechanical connectors are (1) resisting the shear force (V) and tolerating the slip along the tangential direction at the steel-concrete interface; (2) resisting separation and providing pull-out resistance (T) in the normal direction to interface.

As specified in the Euocrode 4 and AISC 360-10, for mechanical connectors, their interfacial shear resistance is determined by the concrete compressive strength, ultimate strength of steel, cross sectional area, and their embedding depth in concrete. Pull-out resistance of connectors (Yan *et al*. 2019b) is governed by embedding depth, cross-sectional area of connectors, and strength of the concrete core. Considering these influencing parameters on shear and tensile resistance of connectors, "Enhanced C-channel" (EC) connectors were developed to enhance the pull-out resistance of the C-channel connector since its one flange is welded to the steel faceplate and the other flange was connected to the opposite steel skin plate by the externally connected "blind blot" or ordinary bolt. Compared with the overlapped headed studs, this type of connector greatly improves the pull-out resistance of the connectors since their tensile separations are partially resisted by the anchoring concrete core and partially directly resisted by the opposite side of steel skin plate. Compared with the friction-welded straight bars in Bi-steel structures and laser-welded connectors, the costing of EC connectors is significantly reduced.

Fig. 2 shows the details of EC connectors. It consists of C-channel connectors and blind bolts or bolts. The construction procedures for DSC structure with EC connectors are as the following;

(1) Welding C-channels to the steel skin plates and reserving holes in flanges for externally connected blind bolts or normal bolts as shown in Fig. 2(b);
(2) Assembling steel skeletons and connecting the blind bolts or bolts from the external of steel skeleton as shown in Fig. 2(c);
(3) Preparing the mould for concrete casting and casting of concrete [See Fig.2(d)];
(4) Curing.

Fig. 3 depicts different components and fabrication procedures of DSCWs with novel enhanced C-channel connectors. The fabrication procedures include welding the C-channel connectors to two external steel faceplates [see

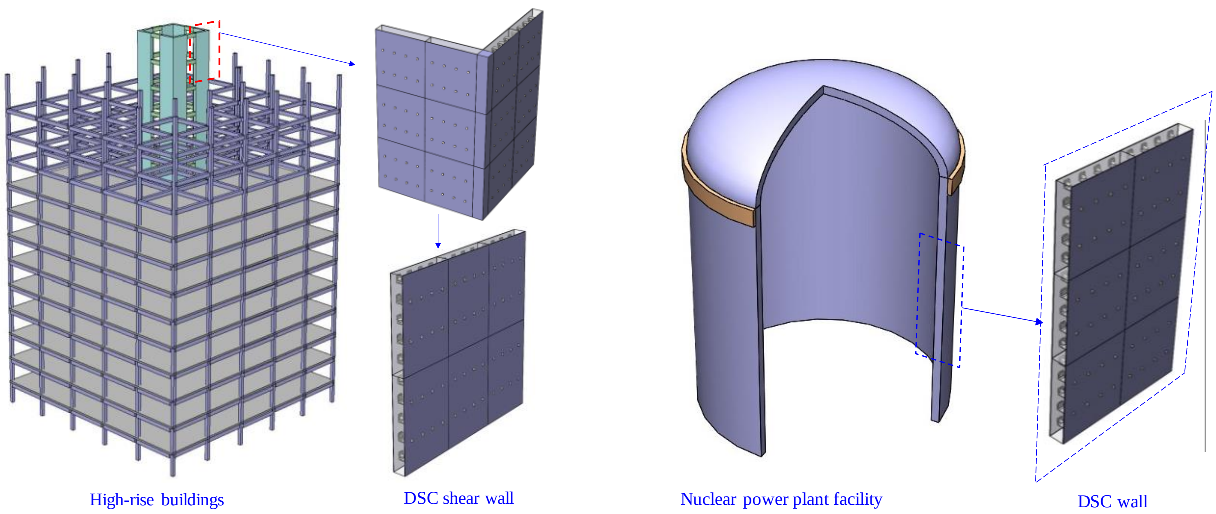

(a) DSC shear wall in high-rise buildings (b) DSC sandwich wall as shielding walls in nuclear power plant

Fig. 1 Applications of DSCWs

Fig. 3(b)], assembling the top and bottom steel faceplates [see Fig. 3(c)], screwing in the bolts from outside of the steel skeleton [see Fig. 3(d)], and casting of concrete [see Fig. 3(e)]. Details of the C-channel connector used in this study is shown in Fig. 3(f).

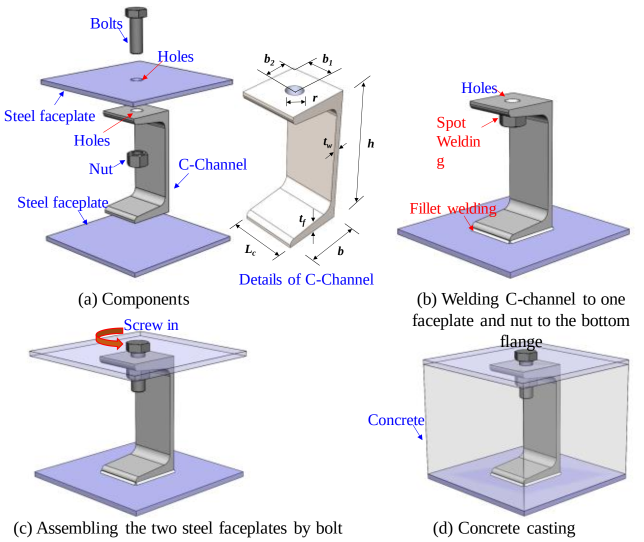

Fig. 2 Details of EC connectors in DSCWs

3. Compressive tests on DSCWs with EC connectors

Since the DSCW with EC connectors was developed as shear walls for buildings and nuclear power plant shielding walls, its compressive behaviours need to be firstly evaluated. A testing program with five large scale specimens was carried out.

3.1 Details of specimens

Fig. 4 illustrates preparation procedures for DSCWs with novel EC connectors. There are totally five DSCWs with EC connectors prepared in this testing program. The selected parameters for this testing program are the direction for layout of the C-channel connector, steel-faceplate (t_s), spacing of C-channels along vertical direction (S_v), spacing of the C-channel connectors along horizontal direction (S_h). Specimen W1 is designed with the controlling parameters. W1 and W2 were designed with different layout of the C-channel connectors. The webs of the C-channel connectors in W1 were put horizontally whilst these webs in W2 were vertically installed. In order to investigate the influence of t_s, specimens W1 and W3 were designed with different thickness of steel skin plate of 2.8 and 4.8 mm, i.e., steel contents of 4.5% and 7.5%, respectively.

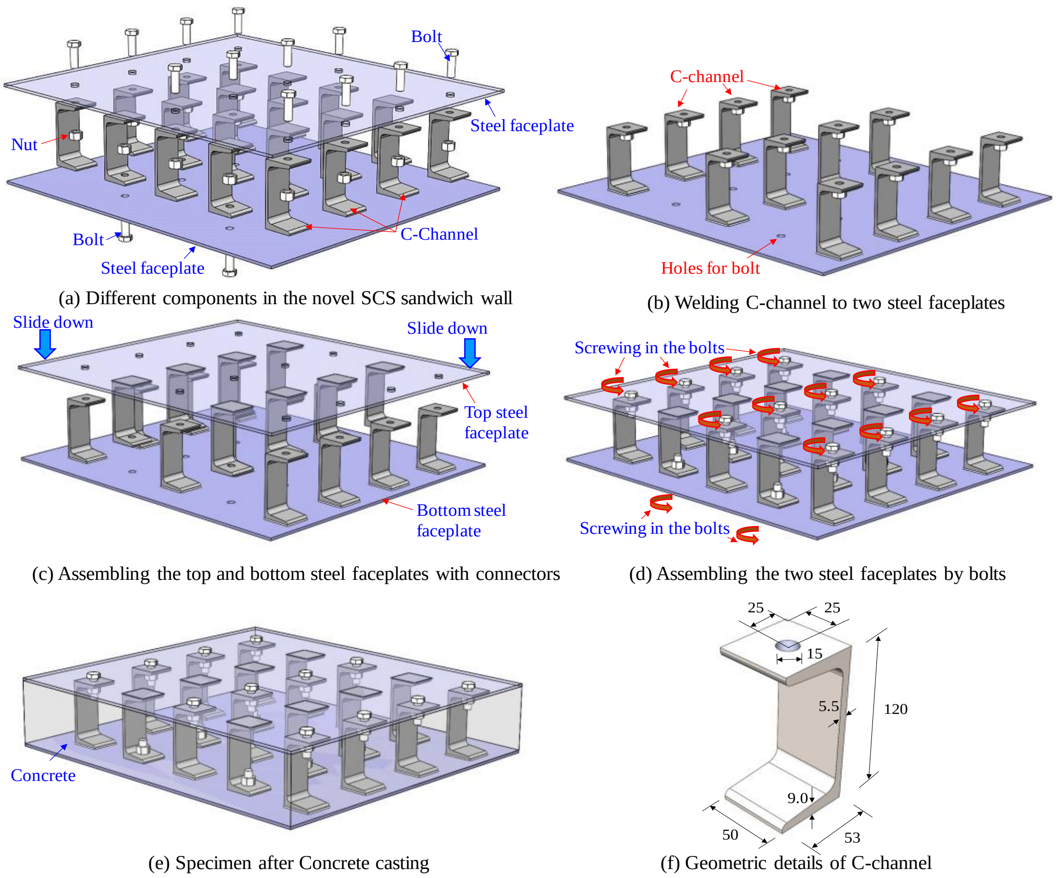

Fig. 3 Fabrication details of DSCW with enhanced C-channel connectors

(a) Prepared steel skeleton (b) Preparing mould for casting of concrete

(c) Casting of concrete (d) Specimen after casting

Fig. 4 Fabrication of DSCWs

As shown in Fig. 5, the depth of core material (t_c), width (B), and height (H) for each DSCW are 120, 600, and 660 mm, respectively. Q235B type of C-channel connectors measure 120 × 53 × 5.5 × 9 × 50 mm^5 in height × flange width × web thickness × flange thickness × flange length, respectively [see Fig. 4(f)]. Its elastic Young's modulus (E_s), yield (f_y) and ultimate (f_u) strengths are 202 GPa, 235 MPa, and 365 MPa, respectively. 2.8 and 4.8 mm-thick Q235 mild steel plates were involved in this study. The f_y and E_s values for 2.8 mm-thick mild steel plates are 235 MPa and 201 GPa, respectively whilst f_y and E_s values for 4.8 mm-thick steel plate are 255 MPa and 203 GPa, respectively. M8.8 grade type of bolts (measuring 14 mm × 40 mm in diameter × height) were used in specimens W1~5, and their yield strengths are 640 MPa.

The compressive strength of the normal weight concrete were obtained from compression tests on three 100 × 100 × 300 mm^3 prisms. The average compressive strength is 53.3 MPa with standard deviations of 3.1 MPa.

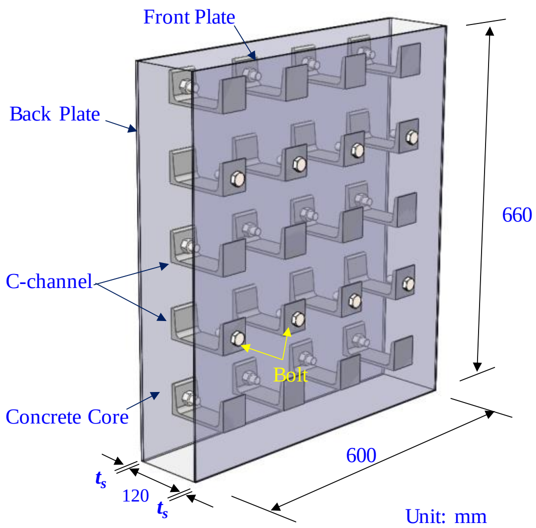

(a) 3D view of W1, W3-5

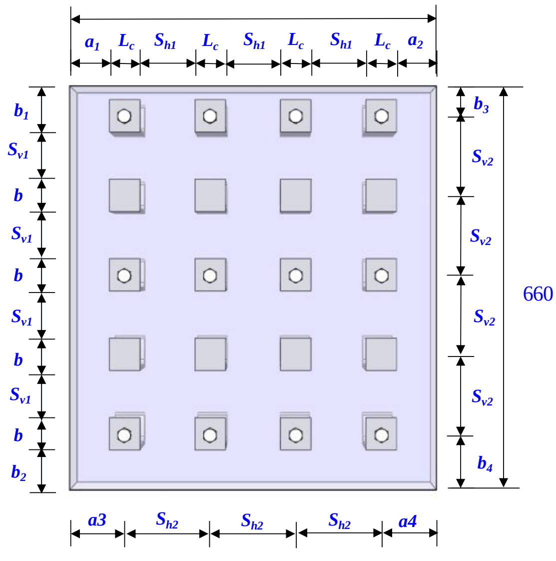

(b) Elevation view of W1, W3-5

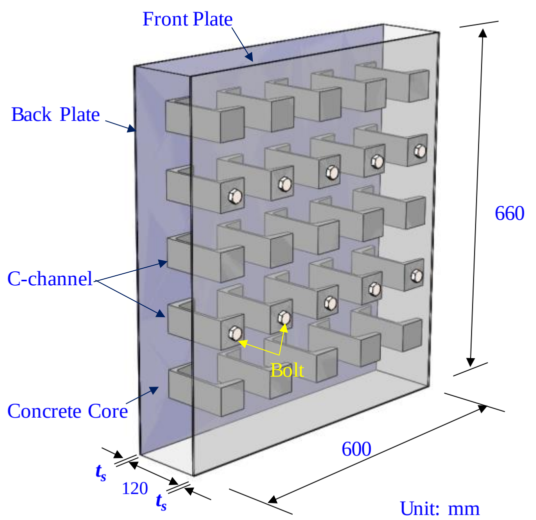

(c) 3D view of W2

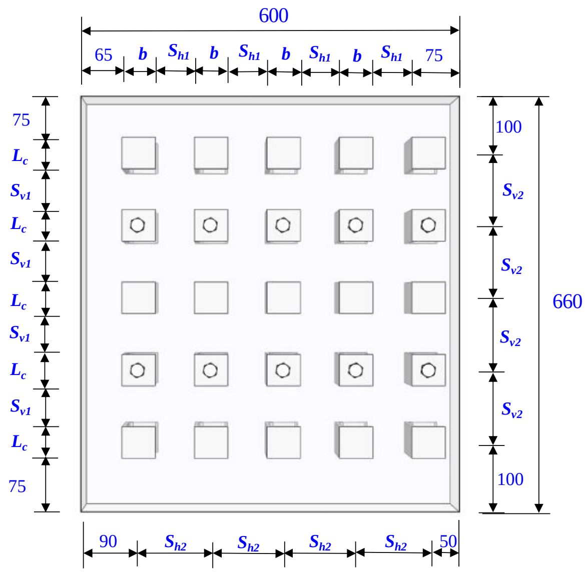

(d) Elevation view of W2

Fig. 5 Geometric details of DSCWs with EC connectors

Table 1 Details and test results of DSCWs with EC connectors

Item	t_c (mm)	t_s (mm)	S_{v1} (mm)	S_{v2} (mm)	S_{h1} (mm)	S_{h2} (mm)	S_{Va} (mm)	S_{ha} (mm)	K_e (kN/mm)	Δ_u (mm)	$\Delta_{85\%}$ (mm)	*DI* Ratio	P_u (kN)	N_{ua} (kN)	P_u/N_{ua}
W1	118.8	2.8	37	90	90	140	90	115	1760	3.53	4.51	1.28	5090	5018	1.01
W2	117.9	3.0	65	115	62	115	90	115	1662	3.99	4.76	1.19	4312	5042	0.86
W3	119.1	4.8	37	90	90	140	90	115	1939	3.58	5.22	1.46	6016	5592	1.08
W4	116.0	2.9	77	130	90	140	130	115	1653	3.46	4.02	1.16	4183	4518	0.93
W5	118.2	3.0	37	90	150	200	90	175	1740	3.08	3.61	1.17	4409	4224	1.04
Mean															0.98
Cov															0.09

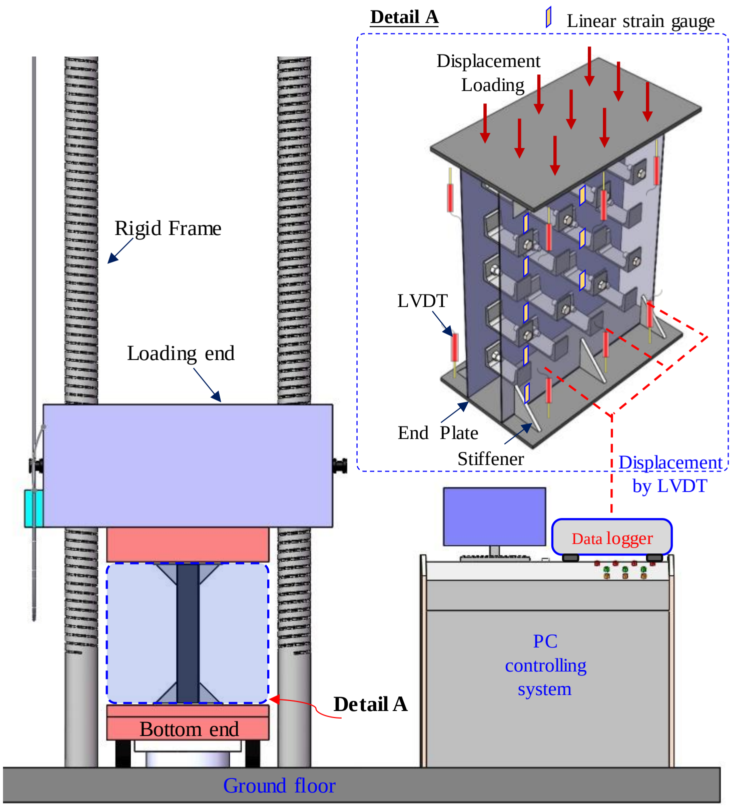

Fig. 6 Test setup

3.2 Test setup and measurements

Compression tests on DSCWs were performed under a 1500-ton hydraulic testing machine in structural lab of Tianjin University as shown in Fig. 6. All the DSCWs were firstly put on the bottom rigid support and loaded on the top end plate by displacement type of loading. 0.05 mm/min was the used loading rate during testing to avoid vibrations. Linear varying displacement transducers (LVDTs) were record the shortening of the DSCW. During the testing, on each end plate of the DSCW, six LVDTs with three on both left and right sides were installed as shown in Fig. 6. Thus, 12 LVDTs in total were used in these compression tests. Including the shortening, this paper also adopted linear strain gauges to measure strains developed in two external steel plates along the height direction. Those measured positions are illustrated in Fig. 6. In addition, both two external steel faceplates were measured at the same positions by those linear strain gauges. More details could be found in Fig. 6. The reaction forces at different loading levels were automatically measured by the testing machine. A data logger as shown in Fig. 6 was used to collect the displacement and reaction force during the testing.

4. Test results

4.1 Failure modes

Failure modes of the DSCW W1~5 are plotted in Fig. 7. For specimen W1, as shown in Fig. 7(a), the first minor buckling of the faceplate at position (1) was observed at the

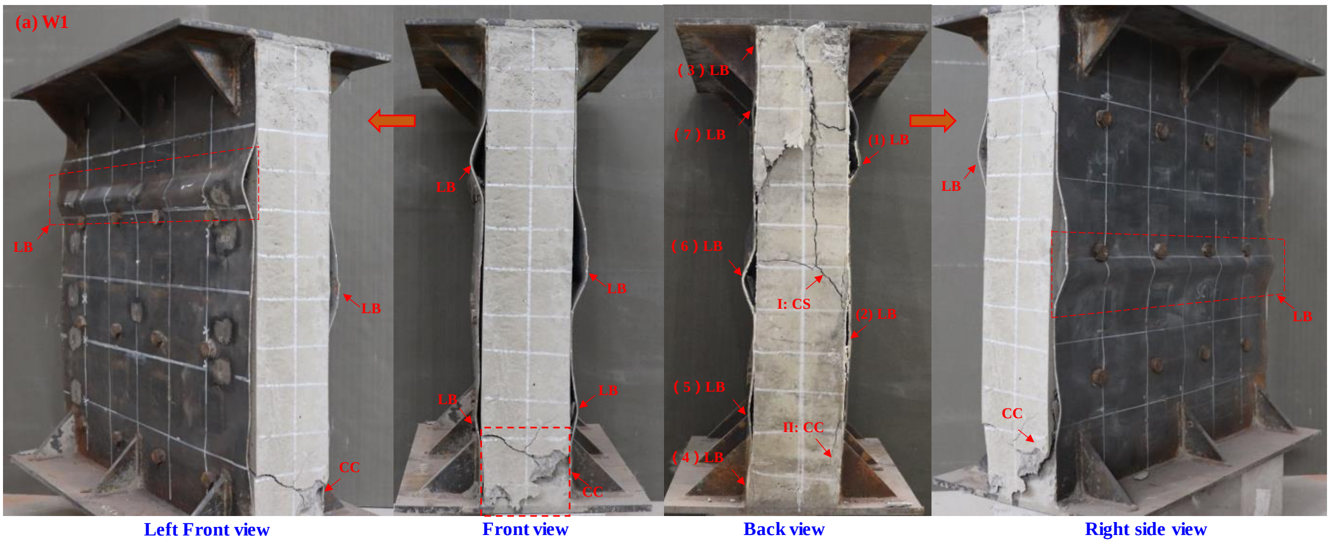

(a) W1

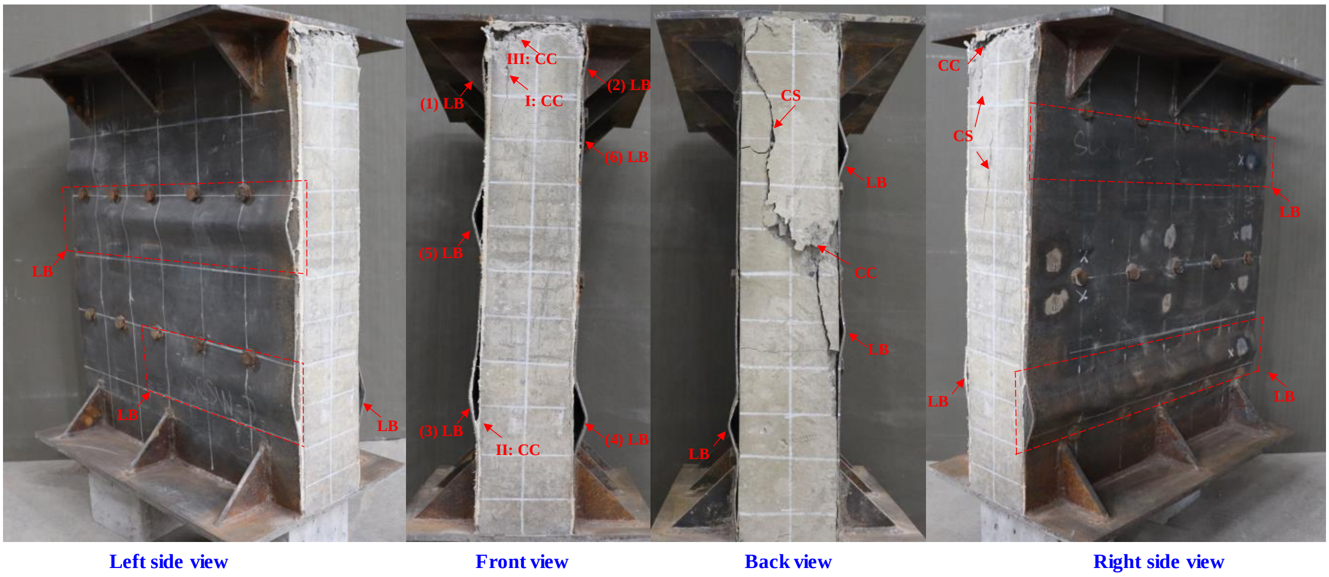

(b) W2

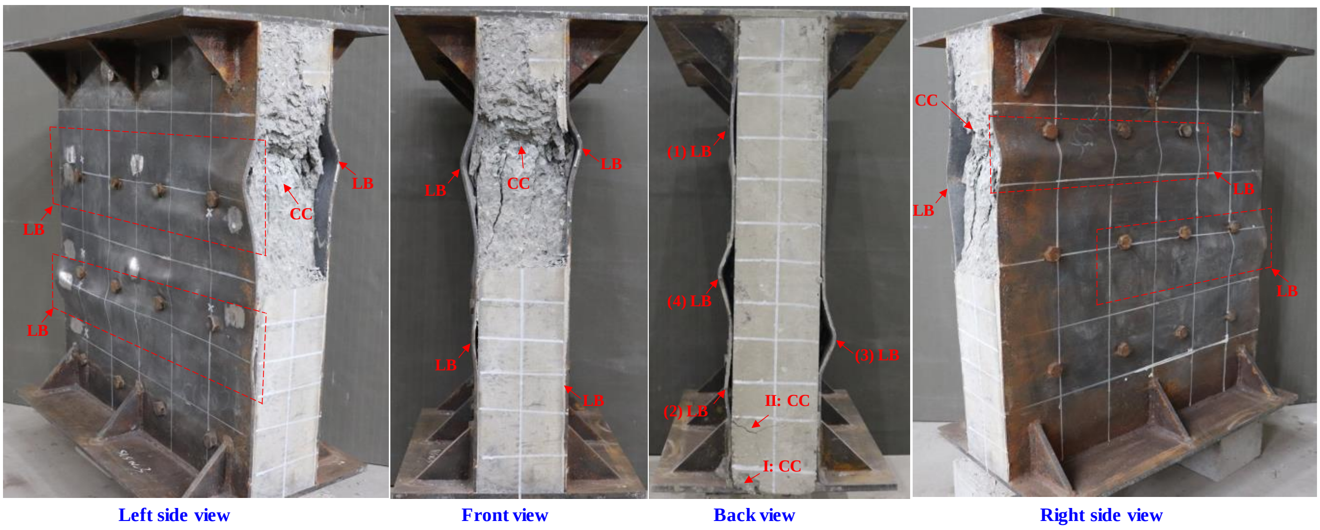

(c) W3

Fig. 7 Failure mode of DSCW with EC connectors

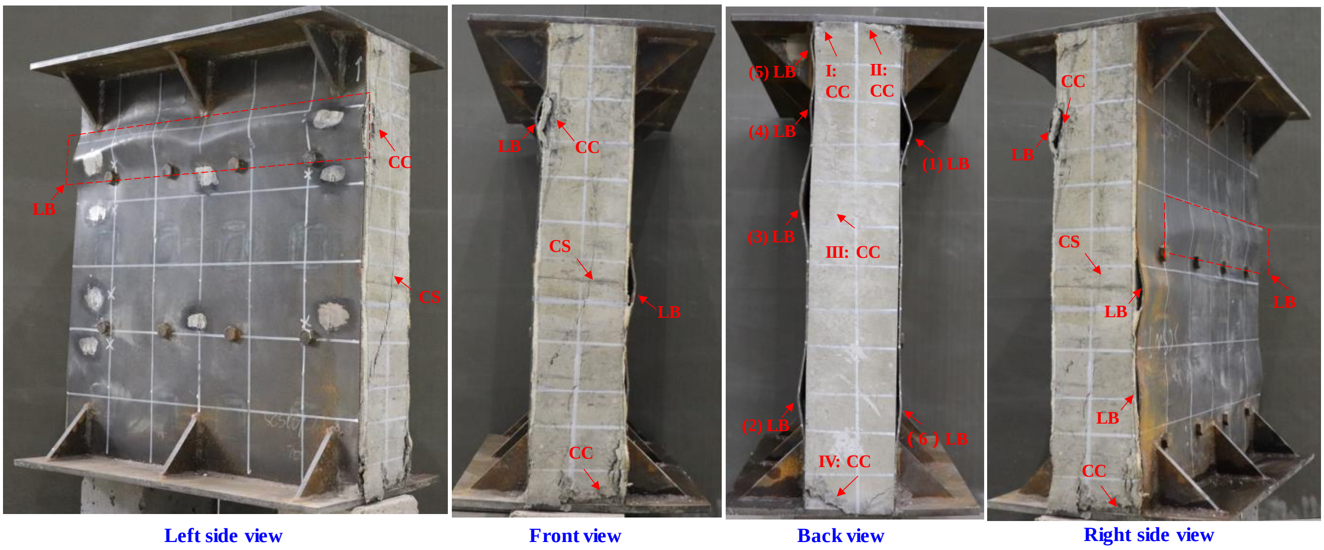

(d) W4

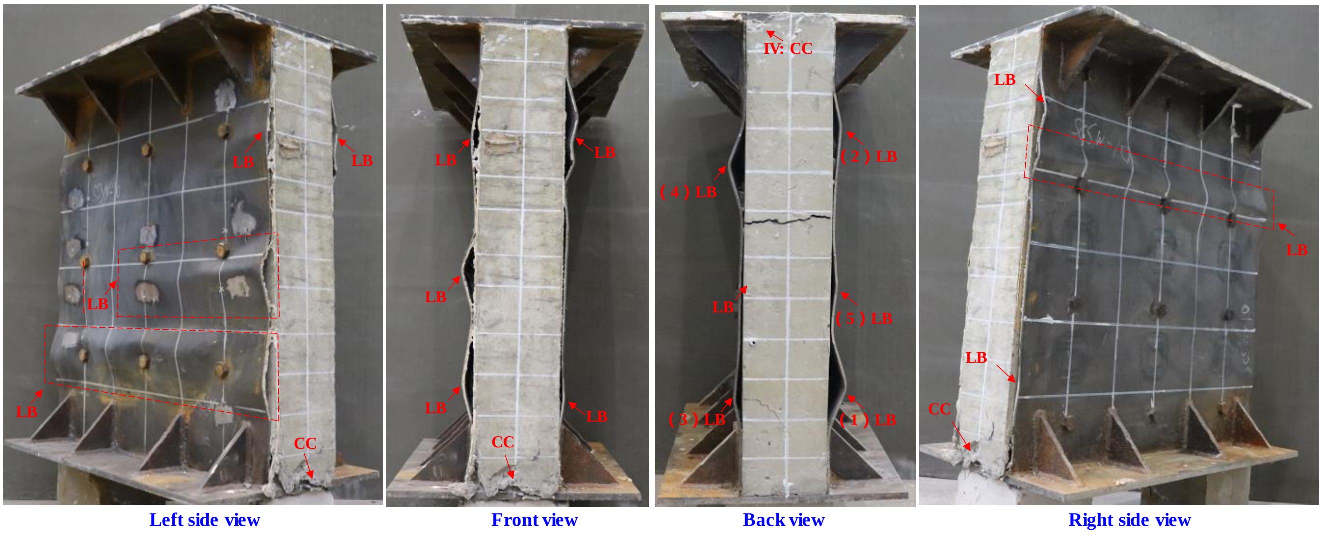

(e) W5

Fig. 7 Continued

loading level of 1352 kN. After that, as the load increases the second minor local buckling in faceplate at position (2) was observed at 1973 kN. After that, local buckling gradually developed in the opposite steel skin plate at location (3) and (4) at compressive load of 2472 kN. Meanwhile, cracks developed in the concrete at potion I [See Fig. 7(a)]. After that major local buckling in faceplate developed and steel skin plate at position (6) and (7) locally buckled as the reaction force equals to 4200 kN. Moreover, the major buckling crossing the whole width of strips in steel faceplates at positions (1) and (6) were observed. Finally, concrete crushing was observed and the specimen achieved its ultimate load carrying capacity. Meanwhile, local buckling crossing the horizontal strip between two arrows of connectors were observed at position (1), (2), and (5)~(7).

Fig. 7(b) depicts failure modes for W2. It shows that as the reaction force (P) increases to 588 kN, slight outward minor buckling occurs at position (1) and (2) near the loading end. After that, as P equals to 1492 kN, cracking of the concrete was observed at position I. Followed, as P equals to 1899 kN, local buckling occurs to steel skin plates at position (3) and (4); meanwhile, vertical cracks at position II can be observed. As P increases to 3420 kN, concrete crushing at local position III can be observed and steel plate at position (5) locally buckled. Major local buckling of the strip at positions (4)~(6) propagated the whole width of the specimen. Finally, concrete crushing at mid-height was observed and the specimen achieved its ultimate compressive resistance.

Fig. 7(c) depicts failure modes for W3. It shows that as P increases to 3018 kN, the cracking and local crushing was observed in the concrete at position I. After that, as P increases to 4222 kN, initiation of major local buckling was observed in the steel faceplate at positions (1) and (2). After that during the period as P increases from 4782 kN to 5320 kN, local buckling of steel faceplates at positions (2) and (4) develops. As P increases from 5893 kN, severe local buckling at position (2) and (4) was observed. Finally, concrete crushing occurred as the W3 achieves its ultimate compressive resistance.

Fig. 7(d) depicts failure modes for W4. It shows that as the applied load P increases to 493 kN, minor local buckling was observed at position (1) and (2). As P increases to 2106 kN, the strips of steel faceplates at position (3) and (4) starts to buckle; meanwhile, the concrete at position III and IV started to crack. As P achieves 2940 kN, concrete at position IV peels off, and major local buckling was observed in faceplate-strip between two rows of C-channels at position (6). Finally, specimen W4 achieved its ultimate compressive resistance of 4183 kN, and it failed in crushing of concrete and buckling of faceplate

Fig. 7(e) depicts failure modes for W5. It shows that minor local buckling occurs to the strips of steel faceplates at positions (1), (2), and (3)~(4) as P increases to 1000 kN, 1200 kN, and 2190 kN, respectively. At the loading level of P = 3900 kN, the outward-buckled horizontal strips of steel faceplates propagate through the width and separated from the concrete core of W5. Finally, W5 failed in concrete crushing (e.g., crushing at position IV) and local buckling of faceplates at peak load of 4409 kN.

4.2 Load-shortening behaviours

Load-shortening (P-Δ) curves of W1~W5 are depicted in Fig. 8. These figures show that all DSCWs with novel enhanced C-channel connectors exhibit a three-stage working manner that consists of linear, nonlinear developing, and after peak recession stage. During the linear stage, it can be found that the reaction compressive force of the specimen increases linearly with the increasing shortening even though occurrences of minor local buckling in the faceplates at several local positions. This implies that the minor local buckling in faceplate does not bring reductions in the initial stiffness of the specimen. At the final point of linear stage, major local buckling in faceplates were observed in W1~W5. In the followed nonlinear stage, the major local buckling continued developing in faceplates, and gradually propagate to the full width between two rows of C-channels. Meanwhile, the concrete core also behaves nonlinearly. Thus, nonlinear behaviour of DSCWs subjected to compression was mainly produced by the nonlinear mechanical properties of the concrete core and development of the major local buckling in faceplates. At the final of nonlinear stage, concrete crushing was observed in all specimens at their ultimate loads. Moreover, due to the developments of the major buckling steel-faceplate strip at different positions, small vibrations may exist in the P-Δ curves. Finally, the DSCW enters recession stage with gradual reducing compressive reaction forces.

4.3 Load-strain behaviours

Load-strain curves at critical positions of the steel faceplates are plotted in Fig. 9. It shows similar three working stages to those in the P-Δ curves. In the first working stage, the strain develops slowly and keeps in linear relationship with the reaction forces. At the end of

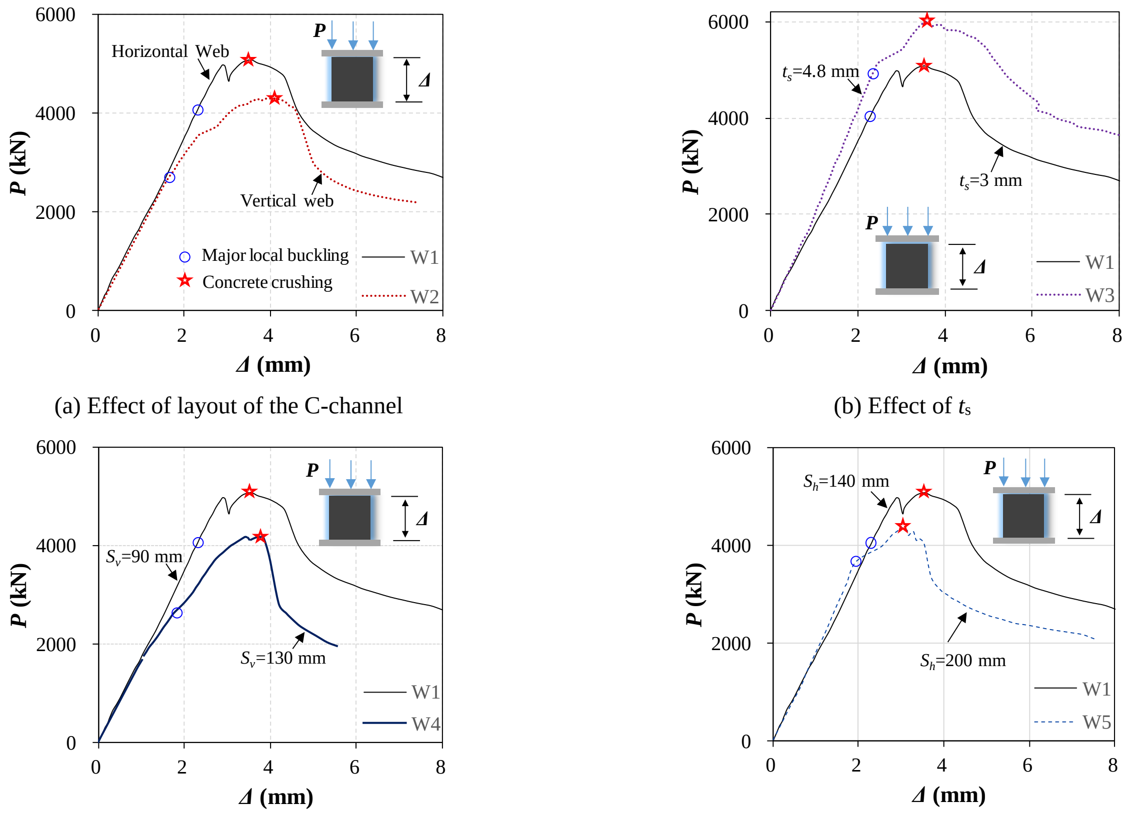

(a) Effect of layout of the C-channel (b) Effect of t_s

(c) Effect of S_v (d) Effect of S_h

Fig. 8 Load versus shortening curves of DSCWs subjected to compression

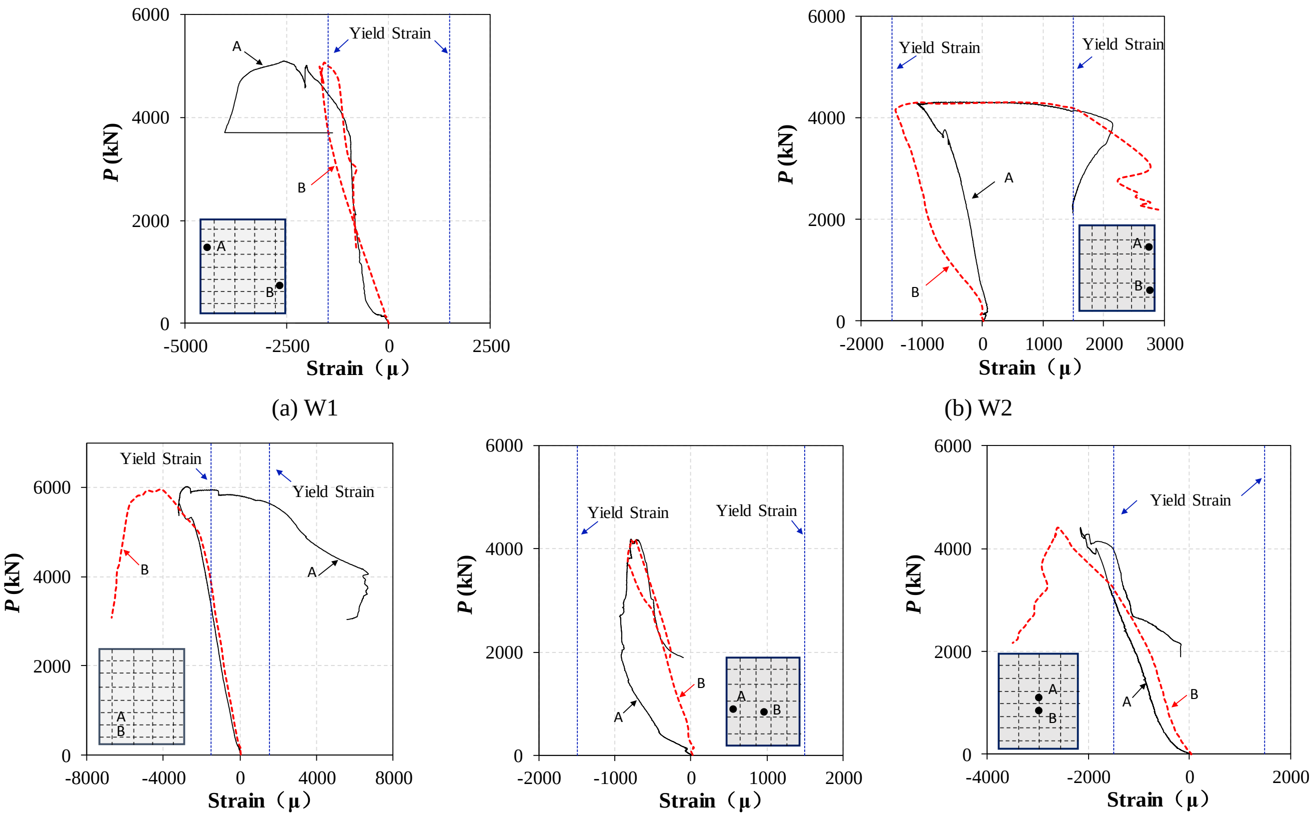

(a) W1 (b) W2

(c) W3 (d) W4 (e) W5

Fig. 9 Load versus strain in steel faceplate curves of DSCW

first working stage, the steel faceplate in specimen W3 and W5 at the measured positions yielded whilst measured strains in steel faceplates of specimens W1, W2, and W4 did not achieve the yielding point. Thus, in nonlinear stage, the nonlinear behaviour of the load-strain curves for W3 and W5 were mainly due to the nonlinear behaviour of the materials and faceplate-local buckling. At this stage, the nonlinear behaviours of load-strain curves for W1~2 and W4 were mainly produced by the faceplate-local buckling. However, at the end of this stage, the five specimen behave in three different manners. The first type is that at the end of the second stage, the steel faceplate yielded, which indicates plastic buckling occurred to the steel faceplates. Specimens W1, W3, and W5 are belonged to this category. Specimen W2 almost achieved plastic buckling in their steel faceplates. Specimen W4 is belonged to the third type characterized by elastic buckling occurred to the steel faceplates.

4.4 Ultimate compressive resistance, initial stiffness, and ductility ratio

Ultimate compressive resistance (P_u) and initial stiffness (K_e) of DSCWs with novel EC connectors are directly determined from those *P*-Δ curves. Finally, these determined K_e and P_u values for DSCWs with novel EC connectors are given in Table 1.

The ductility ratio, *DI*, may be used in this paper to evaluate the ductility of DSCWs with EC connectors. The *DI* ratio equals to the value of displacement corresponding 85% P_u value determined from the recession *P*-Δ curves ($\Delta_{85\%}$) to the displacement at ultimate load carrying capacity (Tao *et al.* 1998), i.e.

$$DI = \frac{\Delta_{85\%}}{\Delta_u} \tag{1}$$

where, *DI* denotes ductility ratio; Δ_u denotes displacement at P_u.

Finally, the *DI* ratios for tests of W1~5 are given in Table 1.

4.5 Discussions

The influences of layout of C-channels, t_s, S_v, and S_h on P_u, K_e, and *DI* ratios were discussion in the following section.

4.5.1 Effect of web direction of C-channels

Since the C-channels could be arranged with its web along the horizontal and vertical direction, W1 and W2 were designed with close quantity of C-channel connectors (e.g., 28 and 25 C-channel connectors were used in W1 and W2, respectively), but with webs in horizontal and vertical directions (See Fig. 5). Fig. 8(a) depicts the influence of web direction on *P*-Δ curves, and Fig. 10(a) plots the influence of web direction for C-channel on P_u, K_e, and *DI*. These figures show that C-channel connectors with horizontally-arranged web generally improve the compressive behaviour of DSCW that increase the P_u, K_e, and *DI* by 18%, 6%, and 8%, respectively. The influences on P_u is more significant than those on K_e and *DI*. However, total amounts of C-channel connectors used in W1 are close to W2, and the slenderness ratios for faceplate for W1 and W2 are about 30. The reduced compressive resistance may be explained by that the vertical web in W2 may produce stress concentration as the specimen subjected to compression, which will lead concrete-core splitting. Thus, it is recommended that C-channel connectors were recommended to be arranged with their webs perpendicular to the axial compressive forces.

4.5.2 Effect of faceplate thickness t_s

Fig. 8(b) shows the influence of t_s on *P*-Δ curves of DSCW with EC connectors. The influences of t_s on P_u, K_e, and *DI* are plotted in Fig. 10(b). These two figures show that increasing the value of t_s improves the compressive behaviours of DSCW. When t_s increases from 3 to 4.8 mm, the P_u, K_e, and *DI* values are increased 18%, 10%, and 14%, respectively. These improvements on the compressive behaviours are mainly due to the increased cross-sectional steel content and the reduced slenderness ratio of faceplate. With the fixed spacing of the C-channel connector of 90 mm, increasing the t_s from 3 to 4.8 mm reduces the slenderness ratio (S_{va}/t_s) from 32.1 to 18.8, which increases the compressive buckling resistance of faceplate. The increased initial stiffness and ductility were due to increased steel content of cross section.

4.5.3 Effect of vertical spacing of C-channels S_v

Fig. 8(c) plots the influence of average vertical spacing of C-channels (S_{va}) on *P*-Δ curves of DSCWs with EC connectors. It shows that the increased S_{va} value generally compromises the compressive behaviour of DSCW. Fig. 10(c) depicts the influences of S_{va} on P_u, K_e, and *DI*. It shows that during the increase of S_{va} from 90 to 130 mm, the P_u value is reduced from 5090 kN to 4183 kN that corresponds to a 18% reduction; meanwhile, the K_e and *DI* were reduced by 6% and 9%, respectively. This implies the influence of S_{va} on K_e is marginal. This is because increasing the S_{va} value from 90 mm to 130 mm reduces the slenderness ratio (S_{va}/t_s) from 32.1 to 46.4 that results in reduced compressive buckling resistance of faceplate. However, K_e is determined by the elastic behaviour of DSCW, and it is not influenced by the slenderness ratio.

4.5.4 Effect of horizontal spacing of C-channels S_h

Fig. 8(d) plots the effect of average horizontal spacing of C-channels (S_{ha}) on *P*-Δ curves of DSCW with EC connectors. It shows that the increased S_{ha} value generally compromises the compressive behaviour of DSCW. Fig. 10(d) depicts the influences of S_{ha} on P_u, K_e, and *DI*. This figure shows that as the S_{ha} increases from 115 to 175 mm, P_u of DSCW is reduced from 5090 kN to 4409 kN with a reduction of 13%. However, the initial stiffness was only reduced by 1% from 1760 kN/mm to 1740 kN/mm. In addition, the DI ratio was reduced by 9%. With the fixed vertical spacing of 90 mm, the slenderness ratio of the steel faceplate was not changed. However, this slenderness ratio is calculated with an assumption that the steel faceplate buckles between two rows of C-channel connectors. This

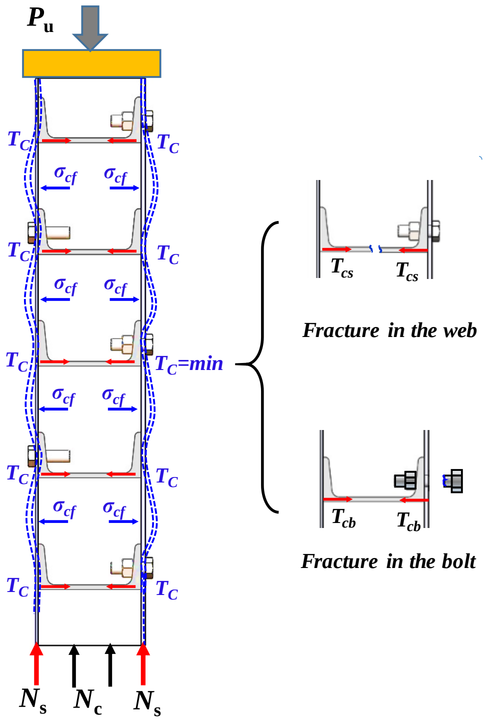

Fig. 11 Failure mode of EC connectors under tension and buckling of steel faceplate in the DSCWs with ECs

assumption only works if sufficient connectors along the horizontal connections were provided. However, if the spacing of the connectors along the horizontal direction was not properly designed, insufficient restraints would result in larger buckling length of the steel faceplates than S_{va}. This can be clearly reflected in bottom left picture in Fig. 7(e), the buckling length of steel faceplate is almost two times of S_{va}. However, this buckling length is much smaller in W1 as shown in Fig. 7(a) since W1 was designed with sufficient horizontal connectors to resist steel faceplate separating from the concrete core. Thus, it should be paid attention to horizontal spacing of C-channels during the design of DSCW with EC connectors. Since S_h does not change the elastic behaviour of faceplate, the initial stiffness was almost unchanged.

5. Analysis on ultimate compressive resistance of DSCWs with EC connectors

5.1 Development of theoretical models

Since all the tested short DSCWs failed in their cross-sectional compression rather than global buckling, the analytical models developed in this manuscript are limited to the cross-sectional failure.

Thus, the ultimate compressive resistance of DSCW with C-channel connectors (N_{ua}) mainly comprises compressive resistance of core material (N_c) and that of steel faceplates (N_s) as the following

$$N_{ua} = N_c + N_s \tag{2}$$

Fig. 11 shows the under compression the core material of the sandwich wall was confined by the external steel skins.

Since the core can expand along the width direction, ignoring the confinement along the width direction, a plane stress case is assumed for DSCW under compression. According the analytical models proposed by Yan *et al.* (2019b), N_c can be calculated as follows

$$N_c = \sigma_{cc} A_c \quad (3)$$

$$\sigma_{cc} = \frac{\gamma + \sqrt{\gamma^2 - 4(1-\alpha_s^2)\left\{\sigma_{cf}^2 - \left[(1-\alpha_s)f_c + \alpha_s \sigma_{cf}\right]^2\right\}}}{2(1-\alpha_s^2)} \quad (4)$$

$$\gamma = (1 + 2\alpha_s^2)\sigma_{cf} + 2(1-\alpha_s)\alpha_s f_c \quad (5)$$

$$\sigma_{cf} = \frac{T_C}{S_{va} S_{ha}} \quad (6)$$

where, σ_{cc} denotes concrete compressive stress accounting confinement of faceplate; A_c is cross-sectional area for core; f_c is concrete compressive strength; σ_{cf} is horizontal confining stress acting on concrete core; α_s denotes yielding coefficient under shear, and 0.19 is used in this paper; T_c denotes tensile strength of C-channel connectors; S_{va} and S_{ha} denote average spacing of connectors along vertical and horizontal direction, respectively.

As pointed out by Yan *et al*. (2019b), EC connectors is belonged to the "direct link" type of connectors in DSC structures, and its tensile resistance can be determined by the minor tensile resistance of C-channel and bolts as the following

$$T_c = min\begin{Bmatrix} T_{cs} = A_{sc}\sigma_{uc} \\ T_{cb} = A_{sb}\sigma_{ub} \end{Bmatrix} \quad (7)$$

where, T_{cs} and T_{cb} denote tensile resistance of C-channel web and anchoring bolt, respectively; A_{sc} denotes area for web cross section in C-channel; A_{sb} denotes cross-sectional area of externally connected bolt.

Test results revealed that two external steel faceplates failed in outward local buckling. Fig. 11 shows the buckling mode of faceplate in DSCW with the EC connectors. Thus, the buckling stress governs their compressive resistance. As pointed by Yan *et al*. (2019b), the compressive resistance for faceplate can be calculated as follows

$$N_s = min\left(\frac{\pi^2 E_s}{12K^2(\eta S_{v,s}/t_s)}, f_{ys}\right) A_s \quad (8)$$

where, K is the coefficient for boundary condition, and herein equals to 0.7; $S_{v,s}$ denotes calculation vertical spacing of the connectors; η denotes the coefficient considering the influence of horizontal spacing of connectors, and equals to 1.0 for sufficient case and equals to 2.0 for insufficient case; A_s denotes cross-sectional area of the two faceplates.

5.2 Validations

Table 1 compares the predicted Nu values with those test values of DSCWs with novel EC connectors. It shows the average test-to-prediction for the five specimens is 0.98 with a coefficient of variation of 0.09. The most unsafe prediction is for W2 with the test-to-prediction ratio of 0.86. The prediction error is mainly produced by the arrangement of the C-channels since the web of the C-channel in W2 were arranged vertically, which induces splitting cracks in the concrete core and the compressive strength of concrete was not fully utilized.

However, limited validations against five test results were carried out on the developed theoretical models. Further validations are still required.

6. Conclusions

This study reports the developments of a type of DSCW with novel EC connectors, and makes pilot research on their compressive behaviours. Five prototype specimens were prepared for compression tests. The main objective of this paper is to investigate the layout of the C-channel connectors on compressive behaviours of DSCW. Including the prototype tests, this study also developed analytical models for ultimate compressive resistance of this novel DSCW. Some conclusions are drawn as the following;

(1) The DSCWs with novel EC connectors failed in local buckling of faceplates and concrete crushing. For specimen with properly designed spacing of EC connectors of 90 mm, steel faceplates failed in plastic buckling whilst for specimens designed with large spacing of connectors of 130 mm, elastic buckling occurred to the steel faceplates at the peak load carrying capacity. Proper spacing of EC connectors should be paid attention in design process of such type of structure.

(2) Subjected to axial compression, DSCWs with novel EC connectors exhibited linear, nonlinear, and recession working stages. The nonlinear working stages were mainly due to nonlinear mechanical properties of steel material and concrete core and developments of faceplate-local buckling. Concrete crushing and faceplate-local buckling of the steel faceplate occurred to the tested five specimens at their peak resistances.

(3) Installing C-channel connectors with their webs along the axial loading direction reduces the compressive resistance of DSCW by 18% compared with sandwich walls designed with web of C-channel connectors installed vertically. The vertically installed web of C-channel connectors induced splitting of concrete that compromised the ultimate compressive resistance of DSCW. It is recommended that the web of C-channel connectors in the DSCWs should be arranged perpendicular to the axial compression direction.

(4) Increasing the thickness of faceplates improves the compressive behaviour of DSCW through enlarging the cross-sectional steel content and faceplate's slenderness ratio. Increasing the thickness of faceplate from 3 to 4.8 mm improves the ultimate compressive resistance, initial elastic stiffness, and

ductility ratio of DSCW by 18%, 10%, and 14%, respectively.

(5) Increasing the vertical spacing of C-channels from 90 to 130 mm reduces the P_u, K_e, and DI ratio of DSCW by 18%, 6%, and 9%, respectively. Moreover, this increased vertical spacing changed the failure mode of faceplate in DSCW from plastic buckling to elastic buckling due to the enlarged slenderness ratio of faceplate.

(6) The horizontal spacing of C-channel connectors needs to be well controlled. Test results showed that insufficient designed spacing of 175 mm doubles the buckling length of faceplate between two vertical arrays of C-channels compared with the specimen with 115 mm in horizontal spacing of connectors, which results in 13% reduction in Pu of DSCW.

(7) Developed analytical models offered reasonable predictions on ultimate compressive resistance of DSCW with novel EC connectors. Theoretical models averagely underestimate the five test results by 2% with a COV of 0.09. Due to the limited validations, analytical models requires further validations.

(8) Current study mainly focused on the prototype developments and geometric details optimization of layout of EC connectors in DSCWs. More experimental parametric studies are still required to make better understanding on the structural behavior of this novel DSCWs.

Acknowledgments

The authors would like to acknowledge the research grant 51608358 received from National Natural Science Foundation of China and Peiyang Scholar Foundation (grant no. 2019XRX-0026) under Reserved Academic Program from Tianjin University for the works reported herein. The authors gratefully express their gratitude for the financial supports.

References

AISC360-10 (2010), Specification for structural steel buildings. American Institute of Steel Construction, Chicago, IL, USA.

Chen, L., Wang, S., Lou, Y. and Xia, D. (2019), "Seismic behavior of double-skin composite wall with L-shaped and C-shaped connectors", *J. Constr. Steel Res.*, **160**, 255-270. https://doi.org/10.1016/j.jcsr.2019.05.033

Eurocode 4 (2004), Design of composite steel and concrete structures—part 1.1: general rules and rules for buildings. European Committee for Standardization; Brussels, Belgium.

Hossain, K.M.A. and Wright, H.D. (2004), "Flexural and shear behaviour of profiled double skin composite elements", *Steel Compos. Struct., Int. J.*, **4**(2), 113-132. https://doi.org/10.12989/scs.2004.4.2.113

Jelovica, J., Romanoff, J. and Klein, R. (2016), "Eigen frequency analyses of laser-welded web–core sandwich panels", *Thin-Wall. Struct.*, **101**, 120-128. https://doi.org/10.1016/j.tws.2016.01.002

Kolsters, H. and Wennhage, P. (2009), "Optimisation of laser-welded sandwich panels with multiple design constraints", *Mar. Struct.*, **22**(2), 154-171. https://doi.org/10.1016/j.marstruc.2008.09.002

Leekitwattana, M., Boyd, S.W. and Shenoi, R.A. (2011), "Evaluation of the transverse shear stiffness of a steel bi-directional corrugated-strip-core sandwich beam", *J. Constr. Steel Res.*, **67**(2), 248-254. https://doi.org/10.1016/j.jcsr.2010.07.010

Liew, J.Y.R. and Sohel, K.M.A. (2009), "Lightweight steel–concrete– steel sandwich system with J-hook connectors", *Eng. Struct.*, **31**(5), 1166-1178. https://doi.org/10.1016/j.engstruct.2009.01.013

Liew, J.Y.R., Sohel, K.M.A. and Koh, C.G. (2009), "Impact tests on steel–concrete–steel sandwich beams with lightweight concrete core", *Eng. Struct.*, **31**(9), 2045-2059. https://doi.org/10.1016/j.engstruct.2009.03.007

Lin, M., Lin, W., Wang, Q. and Wang, X. (2018), "The deployable element, a new closure joint construction method for immersed tunnel", *Tunn. Undergr. Sp. Tech.*, **80**, 290-300. https://doi.org/10.1016/j.tust.2018.07.028

Malek, N., Machida, A., Mutsuyoshi, H. and Makabe, T. (1993), "Steel–concrete sandwich members without shear reinforcement", *Trans. Jpn. Concr. Inst.*, **15**(2), 1279-1284.

Nie, J.G., Hu, H.S., Fan, J.S., Tao, M.X., Li, S.Y. and Liu, F.J. (2013), "Experimental study on seismic behaviour of high-strength concrete filled double-steel-plate composite walls", *J. Constr. Steel Res.*, **88**, 206-219. https://doi.org/10.1016/j.jcsr.2013.05.001

Qin Y., Li, Y.W., Su, Y.S., Lan, X.Z., Wu, Y.D. and Wang, X.Y. (2019a), "Compressive behavior of profiled double skin composite wall", *Steel Compos. Struct., Int. J.*, **30**(5), 405-416. https://doi.org/10.12989/scs.2019.30.5.405

Qin, Y., Li, Y.W., Lan, X.Z., Su, Y.S., Wang, X.Y. and Wu, Y.D. (2019b), "Structural behavior of the stiffened double-skin profiled composite walls under compression", *Steel Compos. Struct., Int. J.*, **31**(1), 1-12. https://doi.org/10.12989/scs.2019.31.1.001

Remennikov, A., Gan, E.C.J., Ngo, T. and Netherton, M.D. (2019), "The development and ballistic performance of protective steel-concrete composite barriers against hypervelocity impacts by explosively formed projectiles", *Compos. Struct.*, **207**, 625-644. https://doi.org/10.1016/j.compstruct.2018.09.060

Sener, K.C., Varma, A.H., Booth, P.N. and Fujimoto, R. (2015), "Seismic behavior of a containment internal structure consisting of composite SC walls", *Nucl. Eng. Des.*, **295**, 804-816. https://doi.org/10.1016/j.nucengdes.2015.07.038

Sohel, K.M.A. and Liew, J.Y.R. (2014), "Behavior of steel–concrete–steel sandwich slabs subject to impact load", *J. Constr. Steel Res.*, **100**, 163-175. https://doi.org/10.1016/j.jcsr.2014.04.018

Tao, Z., Han, L.H. and Zhao, X.L. (1998), *Behaviour of square concrete filled steel tubes subjected to axial compression*, Proceedings of the Fifth International Conference on Structural Engineering for Young Experts, Shenyang, China, pp. 61-67.

Varma, A.H., Malushte, S., Sener, K. and Lai, Z. (2014), "Steel-plate composite (SC) walls for safety related nuclear facilities: design for in-plane force and out-of-plane moments", *Nucl. Eng. Des.*, **269**, 240-249. https://doi.org/10.1016/j.nucengdes.2013.09.019

Xie, M., Foundoukos, N. and Chapman, J.C. (2007), "Static tests on steel–concrete–steel sandwich beams", *J. Constr. Steel Res.*, **63**(6), 735-750. https://doi.org/10.1016/j.jcsr.2006.08.001

Yan, J.B., Liew, J.Y.R. and Zhang, M.H. (2014a), "Ultimate strength behavior of steel-concrete-steel sandwich beams with ultra-lightweight cement composite, Part 1: Experimental and analytical study", *Steel Compos. Struct., Int. J.*, **17**(6), 907-927. https://doi.org/10.12989/scs.2014.17.6.907

Yan, J.B., Liew, J.Y.R., Zhang, M.H. and Wang, J.Y. (2014b), "Ultimate strength behavior of steel-concrete-steel sandwich beams with ultra-lightweight cement composite, Part 2: Finite element analysis", *Steel Compos. Struct., Int. J.*, **18**(4), 1001-1021. https://doi.org/10.12989/scs.2015.18.4.1001
Yan, J.B., Wang, Z. and Wang, T. (2018), "Shear and tensile behaviors of headed stud connectors in double skin composite shear wall", *Steel Compos. Struct., Int. J.*, **26**(6), 759-769. https://doi.org/10.12989/scs.2018.26.6.759
Yan, C., Wang, Y., Zhai, X., Meng, L. and Zhou, H. (2019a), "Experimental study on curved steel-concrete-steel sandwich shells under concentrated load by a hemi-spherical head", *Thin-Wall. Struct.*, **137**, 117-128. https://doi.org/10.1016/j.tws.2019.01.007
Yan, J.B., Wang, Z., Luo, Y.B. and Wang, T. (2019b), "Compressive behaviours of novel SCS sandwich composite walls with normal weight concrete", *Thin-Wall. Struct.*, **141**, 119-132. https://doi.org/10.1016/j.tws.2019.01.051
Yousefi, M. and Ghalehnovi, M. (2017a), "Push-out test on the one end welded corrugated-strip connectors in steel-concrete-steel sandwich structure", *Steel Compos. Struct., Int. J.*, **24**(1), 23-35. https://doi.org/10.12989/scs.2017.24.1.023
Yousefi, M. and Ghalehnovi, M. (2017b), "Finite element model for interlayer behavior of double skin steel-concrete-steel sandwich structure with corrugated-strip shear connectors", *Steel Compos. Struct., Int. J.*, **27**(1), 123-133. https://doi.org/10.12989/scs.2018.27.1.123
Zhang, W. and Atsushi, K.A. (2010), "Behavior of composite segment for shield tunnel", *Tunn. Undergr. Sp. Tech.*, **25**(4), 325-332. https://doi.org/10.1016/j.tust.2010.01.007
Zou, G.P., Xia, P.X, Shen, X.H. and Wang, P. (2016), "Investigation on the .failure mechanism of steel-concrete steel composite beam", *Steel Compos. Struct., Int. J.*, **20**(6), 1183-1191. https://doi.org/10.12989/scs.2016.20.6.1183

DL

Appendix I

Abbreviations

COV	coefficient of variation
DSC	double skin composite
DSCW	double skin composite walls
DSCW-EC	double skin composite walls with novel enhanced C- channel connectors
EC	enhanced C-channel
LVDT	linear varying displacement transducer

Nomenclature

A_c	Cross-sectional area of core
A_s	Cross-sectional area of the two faceplates
A_{sb}	Cross-sectional area of externally connected bolt
A_{sc}	Cross-sectional area of the web in C-channel
DI	Ductility ratio (or index)
K	Coefficient for boundary condition
K_e	initial stiffness
N_{ua}	Ultimate compressive resistance by theoretical model
N_c	Compressive resistance of core material
N_s	Compressive resistance of steel faceplates
P	Applied load
P_u	Ultimate compressive resistance
S_v	Spacing of the C-channel connectors along vertical direction
S_{va}	Average vertical spacing of C-channel connectors
$S_{v,s}$	Calculation vertical spacing of the connectors
S_h	Spacing of the C-channel connectors along horizontal direction
S_{ha}	Average horizontal spacing of C-channel connectors
T	Tensile resistance of connectors
T_c	Tensile strength of C-channel connectors
T_{cb}	Tensile resistance of anchoring bolt
T_{cs}	Tensile resistance of C-channel web
V	Shear resistance of connectors
f_c	Concrete compressive strength
f_{ys}	Yield strength of steel faceplate
t_c	Thickness of concrete core
t_s	Thickness of steel skin plate
Δ	Deflection
Δ_u	Displacement at P_u
$\Delta_{85\%}$	Displacement corresponding 85% P_u
α_s	denotes yielding coefficient under shear
σ_{cc}	Concrete compressive stress considering confinement of faceplate
σ_{cf}	Horizontal confining stress for concrete core
η	Coefficient considering the influence of horizontal spacing of connectors